Langmuir

Article

Conformation of Adsorbed Comb Copolymer Dispersants

Robert J. Flatt, Irene Schober, Elie Raphael, Ce#dric Plassard, and Eric Lesniewska

Langmuir, **2009**, 25 (2), 845-855• DOI: 10.1021/la801410e • Publication Date (Web): 16 December 2008

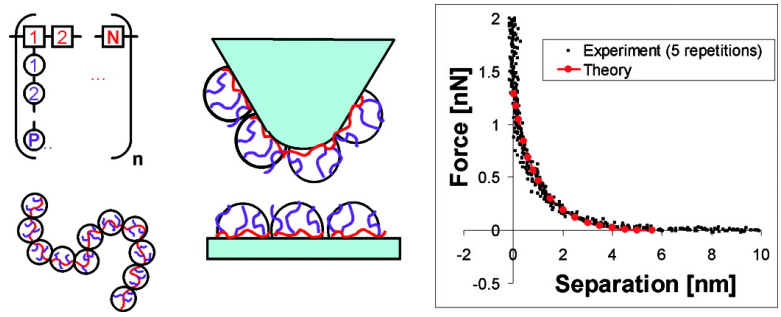

More About This Article

Additional resources and features associated with this article are available within the HTML version:

- Supporting Information
- Access to high resolution figures
- Links to articles and content related to this article
- Copyright permission to reproduce figures and/or text from this article

View the Full Text HTML

Langmuir is published by the American Chemical Society. 1155 Sixteenth Street N.W., Washington, DC 20036

Conformation of Adsorbed Comb Copolymer Dispersants

Robert J. Flatt,*,† Irene Schober,† Elie Raphael,‡ Cédric Plassard,§ and Eric Lesniewska§

Sika Technology, CH-8048 Zürich, Switzerland, UMR CNRS Gulliver 7083, ESPCI, 10 rue Vauquelin, 75231 Paris Cedex 05, and Institute Carnot Bourgogne UMR CNRS 5209, University of Bourgogne, F-21078 Dijon, France

Received May 7, 2008. Revised Manuscript Received October 3, 2008

Comb copolymers with an adsorbing backbone and nonadsorbing side chains can be very effective dispersants, particularly when a high ionic strength strongly penalizes electrostatic stabilization. For this reason, they have become essential components of concrete over the past decade. This article examines the steric hindrance characteristics of such polymers through the use of atomic force microscopy (AFM) on calcium silicate hydrate, the main hydration product of Portland cement. It is found that solution and surface properties (hydrodynamic radius, radius of gyration, surface coverage, steric layer thickness) and force−distance curves obtained during AFM measurements can be well described by a scaling approach derived in this paper. This represents the first real quantitative step in relating these properties directly to the molecular structure of such comb copolymer dispersants.

I. Introduction

Polymeric dispersants play an important role in improving the rheological behavior of concentrated particle suspensions in many industrial processes such as ceramic slurry processing (slip casting, tape casting, filter pressing), paints, cement and concrete placement, cosmetics, and pharmaceutical formulations. Comb copolymers with an adsorbing backbone and nonadsorbing side chains can be very effective dispersants for such systems, particularly when the ionic strength is high. This is the case of concrete, where these polymers have become widely used over the past decade for greatly improving workability, strength, and durability.[1] Other particulate suspensions where these dispersants have been reported to be effective include barium titanate,[2] concentrated cemented carbide,[3] magnesia,[3] limestone,[4] and silica.[5]

In the field of concrete, dispersants are generally referred to as superplasticizers. The comb copolymers of concern in the present study are polycarboxylate esters (PCEs).[1,6] They are composed of comb copolymers with an adsorbing linear anionic backbone (typically a polyacrylate or polymethacrylate) as well as nonadsorbing side chains (typically polyalklene oxides. They are known to adsorb on cement grains[7] and induce steric hindrance between surfaces,[8−10] which reduces or suppresses otherwise attractive interparticle van der Waals forces[11] or ion correlation forces.[12] With such polymers, the role of electrostatic forces in the repulsion is accepted to be negligible[13] or at best a complimentary second-order contribution.[6]

It is expected that longer side chains are more effective in that they keep particles at a larger separation distance so the residual interparticle forces are weaker.[9] In fact, calculations suggest that already with thin adsorbed layers, the interparticle force becomes repulsive as soon as layers begin to overlap.[14] Consequently, the maximum attractive force relevant for rheology depends directly on the thickness of the adsorbed layer and thereby on adsorbed polymer conformation. Recently, atomic force microscopy (AFM) has been used to study such admixtures on the surface of magnesium oxide taken as an inert surface meant to represent cementitious materials.[15,16] Results suggest that the side chains are coiled rather than stretched,[15] which contrasts with the typical sketches broadly used to represent the adsorbed state of these polymers (but not based on any direct evidence).

It was argued that this coiling leads to values of layer thickness that scale with the three-fifths power of side-chain length.[17] This result is known for well-spaced and end-grafted linear chains in good solvent.[18] The argument for this analogy is that although side chains are close to one another along the backbone, the

* Corresponding author.
† Sika Technology.
‡ UMR CNRS Gulliver 7083, ESPCI.
§ University of Bourgogne.

(1) Ramachandran, V. S.; Malhotra, V. M.; Jolicoeur, C.; Spiratos, N. *Superplasticizers: Properties and Applications in Concrete*; Ministry of Public Works and Government Services: Ottawa, ON, Canada, 1998.
(2) Kirby, G. H.; Harris, D. J.; Li, Q.; Lewis, J. A. *J. Am. Ceram. Soc.* **2004**, *87*(2), 181–186.
(3) Laarz, E.; Kauppi, A.; Andersson, K. M.; Kjeldsen, A. M.; Bergström, L. *J. Am. Ceram. Soc.* **2006**, *89*(6), 1847–1852.
(4) Sakai, E.; Kawakami, A.; Daimon, M. *Macromol. Symp.* **2001**, *175*(1), 367–376.
(5) Whitby, C. P.; Scales, P. J.; Grieser, F.; Healy, T. W.; Kirby, G.; Lewis, J. A.; Zukoski, C. F. *J. Colloid Interface Sci.* **2003**, *262*(1), 274–281.
(6) Flatt R. J. In *Polymers in Particulate Systems: Properties and Applications*; Hackley, V. A., Somasundaran, P., Lewis, J. A., Eds.; Marcel Dekker: New York, 2001; Chapter 9.
(7) Schober, I.; Maeder, U. In *Proceedings of the 7th Canmet/ACI International Conference on Superplasticizers and Other Chemical Admixtures in Concrete*; Malhotra, V. M., Ed.; Berlin, October 20−23, 2003; American Concrete Institute: Framington Hills SP-217, 2003; pp 453−448.
(8) Sakai, E.; Daimon, M. In *Materials Science of Concrete IV*; Skalny, J. P., Mindess, S., Eds.; The American Ceramic Society: Westerville, OH, 1995; pp 91−111.
(9) Yoshioka, K.; Sakai, E.; Daimon, M. *J. Am. Ceram. Soc.* **1997**, *80*(10), 2667–2671.
(10) Kirby, G. H.; Lewis, J. A. *J. Am. Ceram. Soc.* **2004**, *87*(9), 1643–1652.
(11) Flatt, R. J. *Cem. Concr. Res.* **2004**, *34*, 399–408.
(12) Van Damme, H. In *Encyclopedia of Surface and Colloidal Science*; Marcel Dekker Inc.: New York, 2002; pp 1087−1103.
(13) Uchikawa, H.; Hanehara, S.; Sawaki, D. *Cem. Concr. Res.* **1997**, *27*(1), 37–50.
(14) Flatt, R. J. *Mater. Struct.* **2004**, *27*(269), 289–300.
(15) Kauppi, A.; Andersson, K. M.; Bergström, L. *Cem. Concr. Res.* **2005**, *35*, 133–140.
(16) Kauppi, A.; Banfill, P. F. G.; Bowen, P.; Galmiche, L.; Houst, Y. F.; Lafuma, F.; Mäder, U.; Perche, F.; Petersen, B. G.; Reknes, K.; Schober, I.; Siebold, A.; Swift, D. In *Proceedings of the 11th International Conference on Cement Chemistry*; Sheath, J., Ed.; Durban, South Africa; ISBN: 0-9584-0858-0(CD-ROM); May 11−16, 2003; pp 528−537.
(17) Kjeldsen, A. M.; Flatt, R. J.; Bergström, L. *Cem. Concr. Res.* **2006**, *36*, 1231–1239.
(18) De Gennes, P. G. *Adv. Colloid Interface Sci.* **1987**, *27*, 189–209.

10.1021/la801410e CCC: $40.75
Published on Web 12/16/2008

surface area available per side chain is much larger and in the range allowing them to assume the mushroom conformation.[17]

With the use of the scaling relation mentioned above and a first-principle yield stress model for particulate suspensions,[19] it was possible to account for the consolidation of magnesium oxide suspension dispersed with such polymers. Thus, there appears to be true possibilities of predicting, at least in a scaling approach, some aspects of the rheological behavior of particulate suspensions, provided the adsorbed polymer conformation is known.

This result is very encouraging and calls for the measurement of adsorbed conformation of superplasticizers in cementitious systems. This was attempted in the past,[13] but results led to values of layer thickness about 1 order of magnitude larger than the polymer dimension, indicating a probable artifact due to the mineral reactivity.[20] As mentioned above, measurements on model systems of MgO have already been reported.[15,16] These results present some limitations in that the MgO surface is not completely inert[21] and a pH of 10 was used, whereas as cementitious system lay rather around 12.5. The use of calcium silicate hydrate, the main hydrate of cement, represents a model systems even closer to true cementitious systems. Indeed, it is the main hydrate of cement. Furthermore, recent developments have made it possible to prepare surfaces of this mineral in ways that are suitable for using AFM as a colloidal probe.[22,23]

In this paper, we have made use such colloidal probe experiments to determine the adsorption conformation and steric hindrance induced by a wide range of comb copolymers with varying side-chain lengths, grafting densities, and backbone lengths. Schematically the paper is organized in three parts. First, there is a presentation of the experimental results. Second, different models of polymers in solution and adsorbed conformation are presented, derived, and discussed. Third, this model is used to derive a theoretical expression for the steric hindrance force. This expression is shown to successfully capture the main parametric dependences, indicating that the question of conformation of comb copolymer on such surfaces is largely resolved.

II. Materials and Methods

The experimental procedure consisted of measuring the interaction forces acting between a probe covered by calcium silicate hydrate (C−S−H) nanoparticles and C−S−H substrate. C−S−H nanoparticles ($60 \times 30 \times 5$ nm^3) were partially recrystallized by Ostwald ripening by long time equilibrium in saturated calcium hydroxide solution in order to obtain an atomically flat C−S−H substrate.[18] We have used these C−S−H substrates to study the adsorption of different polymers using an atomic force microscope. Indeed, some experimental conditions prove to be essential: the probe and substrate should not react with the solution in order to ensure the stability and reproducibility of force measurements. Moreover, the roughness of the substrate must be substantially lower than the layer thickness of the adsorbed polymers. On 145 different C−S−H substrates, the mean roughness measured on 33 different locations were, respectively, 0.59 ± 0.10 nm on 0.25 μm^2 area and 1.16 ± 0.18 nm on 1 μm^2.

II.1. Materials. *II.1.1. Polymers.* Polymers were produced by radical copolymerization. The ratios of methacrylic acid to polyalkyleneglycol methacrylate (C/E) were varied between 2 and 21, the side chains between 500 and 10 000 g/mol, and the backbone between 5300 and 30 000 g/mol (Table 1). The polymers were purified by ultrafiltration with membranes having size exclusions of 1−10 kD, depending on the size of the side chains.

Table 1. Properties of the Polymers Used[a]

polymer	side chain g/mol	C/E	MW BB g/mol
S1	550	2	6000
S2	750	2.5	6000
S3	1000	2.1	7000
S4	1000	3	30 000
S5	1000	8.3	14 000
S6	2000	3	5300
S7	2000	5.9	6000
S8	5000	5.9	7000
S9	5000	13	5300
S10	10 000	21	7000

[a] C/E indicates the ratio of carboxylate to ester groups in the polymer.

Solutions of these polymers were prepared by dissolution in a 5 mM calcium hydroxide solution to obtain 1, 10, and 100 mg/L polymer solutions.

II.1.2. AFM Substrate and Probe Preparation. To get flat C−S−H surfaces in chemical equilibrium with solutions, a freshly cleaved $\{10\bar{1}4\}$ face of calcite was immersed in a sodium silicate solution ($[SiO_2]/[Na_2O] = 0.33$, $[SiO_2] = 0.5$ mol·L^{-1}, pH = 14.2). Precipitation of C−S−H on the calcite cleavage plane was by heterogeneous nucleation from calcium ions provided by the calcite dissolution and silicate and hydroxide ions contained in the solution. The C−S−H growth on calcite gave aggregation of C−S−H nanoparticles of approximately 5 nm height and a developed face of 60 nm by 30 nm.[18] Then the calcite surface covered by C−S−H was immersed in calcium hydroxide solution with a concentration of 5 mmol/L. After 1 month, the calcite surface is covered by smooth C−S−H domains on a micrometer scale formed by Ostwald ripening,[24] thus smoothing out the influence of roughness on force measurements (see Figure 1).

Pyramidal silicon nitride Si_3N_4 tips fixed to commercial triangular cantilevers, double-side Au-coated with a measured spring constant ranging from 0.12 to 0.6 N·m^{-1} (Veeco Co., CA), were used. In order to obtain C−S−H coverage, the silicon nitride tips, which are naturally covered by a thin layer of silica (∼5 nm thick), were immersed in a large volume ($V = 50$ mL) of a saturated calcium hydroxide solution during 48 h. Under these conditions, C−S−H precipitates on the extremity of the tip from the silicate ions provided by the dissolution of silica in the alkaline medium and from the calcium and hydroxide ions from the solution (Figure 2). After complete consumption of the silica layer, the probe was also rendered nonreactive, as long as the silicon nitride bulk was protected from oxidation. EDS analysis on the tip confirmed that the deposited material is C−S−H.[23]

II.2. Methods. *II.2.1. Imaging.* AFM measurements were performed using a commercial AFM (Nanoscope IIIa Quadrex, Veeco Co., Santa Barbara, CA). All images were acquired in glovebox exempt of CO_2 using contact mode AFM or oscillating mode (tapping mode (TM) AFM) with the D-type scanner (12 μm) and the J-scanner (150 μm). For contact mode or TM-AFM mode imaging, V-shaped silicon nitride cantilevers with a nominal spring constant of 0.03−0.36 N/m (Veeco Co.) were used. In order to remove contaminants, the tips were exposed to UV/ozone for 10 min, allowing the removal of the hydrocarbons. For each tip used, the sensitivity response was determined from amplitude calibration plots on glass coverslips. By measuring the thermal noise of the different cantilevers, the associated spring constant was estimated. In contact mode, the height image reflects the topography, whereas the deflection image (i.e., error signal mode) reflects the topographical variation and better contrast. Magnifications of ×200 000 revealed enough details of the morphology and surface adsorption kinetics. On several specimens, surface measurements were made using the section analysis module

(19) Flatt, R. J.; Bowen, P. *J. Am. Ceram. Soc.* **2006**, *89*(4), 1244–1256.
(20) Flatt, R. J.; Houst, Y. F. *Cem. Concr. Res.* **2001**, *31*(8), 1169–1176.
(21) Perche, F. Adsorption de polycarboxylates et de lignosulfonates sur poudre modèle et ciments. Ph.D. Thesis No. 3041, EPFL, Lausanne, Switzerland, 2004 (downloadable at http://library.epfl.ch/thesis/?nr=3041).
(22) Lesko, S.; Lesniewska, E.; Nonat, A. M.; Mutin, J.-C.; Goudonnet, J. P. *Ultramicroscopy* **2001**, *86*, 11–21.
(23) Plassard, C.; Lesniewska, E.; Pochard, I.; Nonat, A. *Langmuir* **2005**, *21*, 7263–7270.
(24) Plassard, C.; Lesniewska, E.; Pochard, I.; Nonat, A. *Ultramicroscopy* **2004**, *100*, 331–338.

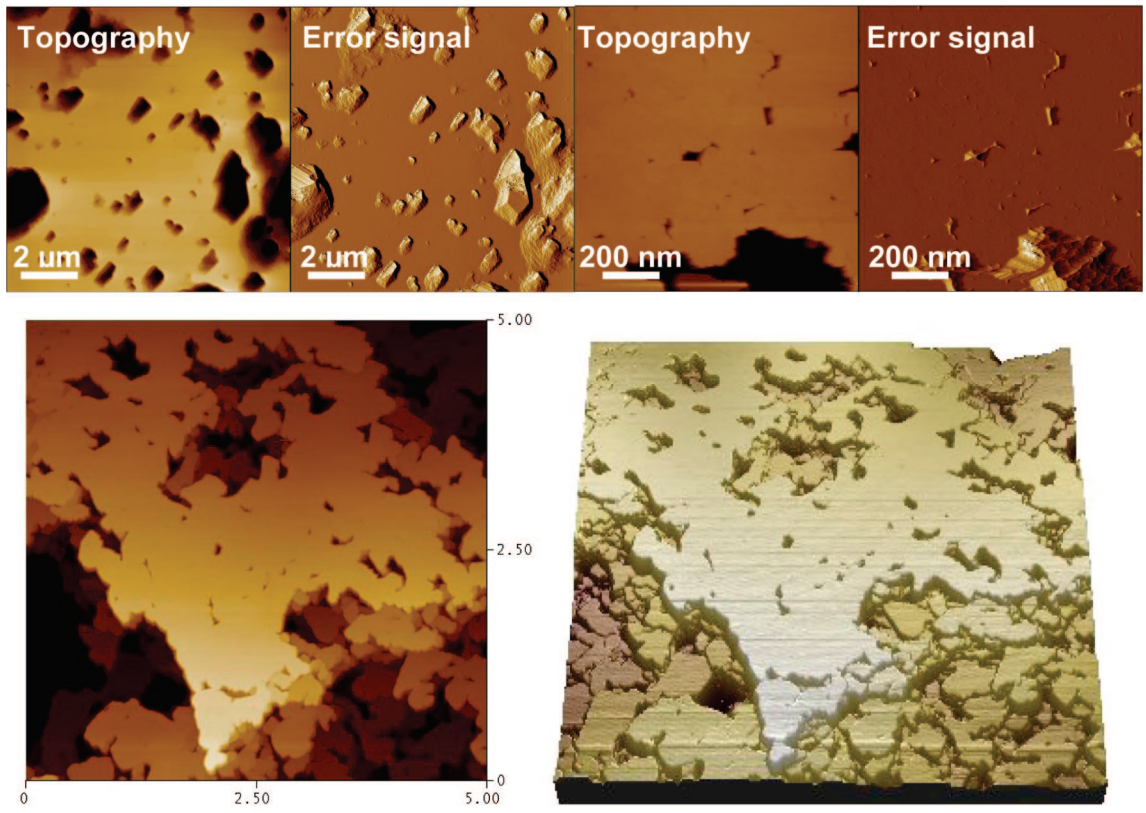

Figure 1. Atomic force microscopic images of a crystallized area of C−S−H obtained on a calcite monocrystal after equilibrium in solution (see text for details). Upper left images (2D and error signal) size: 10 μm. Upper right images (2D and error signal) size: 1 μm. Lower images (2D and 3D) size: 5 μm. Common relative height: 100 nm.

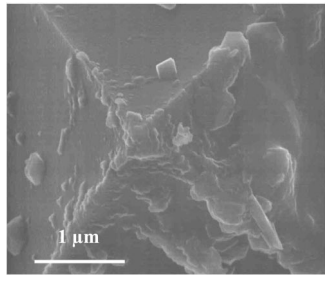

Figure 2. Scanning electron microscopic image of a silicon nitride tip after immersion during 48 h in saturated calcium hydroxide solution: C−S−H nanoparticles are mainly precipitated on the edge and the top of the pyramid.

of the AFM software. This module permits the selection of one or more sections of the image and the performance of various measurements, both in horizontal and vertical plane. Surface roughness is defined as the standard deviation of the Z values within the given area and is calculated using

$$R_q = \sqrt{\frac{\sum (Z_i - Z_{\text{average}})^2}{N}}$$

where Z_{average} is the average of the Z values, Z_i is the current Z value, and N is the number of points (512 × 512) within the given area (1 μm^2).

II.2.2. Force Measurements. Cantilevers with low spring constants have been chosen to be sufficiently sensitive to forces in liquid. In solution, the rate of the vertical motion performed during the approach−retract cycles was lowered to 25 nm·s^{-1} to avoid significant viscous forces from medium. However, in each case first measurements are performed with large displacements (1 μm). In these conditions, the probe and the substrate are kept in contact for 2 s. The maximum force applied by the cantilever (spring constant of 0.6 N·m^{-1}) reaches 10−20 nN. In the compliance regime, the deflection was always equal to the displacement without any instability proving there is no other interaction regime at shorter distance. Interaction forces were obtained with the usual calibration process in order to transform experimental cantilever deflection curves as a function of the vertical scanner displacement Δz into force−distance curves.[25] With the use of the slope of the retraction deflection curves in the contact region, the cantilever deflection is then converted into a force using Hooke's law:

$$F = -k\Delta z \qquad (1)$$

where k is the stiffness constant of the AFM cantilever used, determined by resonant frequency method or thermal noise analysis. Force curves obtained give the force F (nN) against the tip−sample separation (nm).

All experiments were performed in a CO_2-free glovebox purged by 10 successive nitrogen gas introductions and vacuum pumpings in order to prevent carbonation of hydroxide solutions. For studies in aqueous solutions, an adapted commercial fluid cell was used which was coated by parylem C to make it resistant at high pH. The temperature of the surrounding wall was maintained at 25 °C, and humidity was controlled in order to avoid evaporation of the solution.

II.2.3. Polymer Adsorption and Force Curve Interpretation. A volume of 250 μL of test solution was deposited on the plane substrate of C−S−H. The polymer adsorption was carried out with an equilibrium time of 15 min. For each experiment, statistics of over 50 force measurements were established by recording force curves on 50 different locations from each sample. This was done each time before and after polymer adsorption.

On each curve, the distance at which the force begins to deviate significantly from zero was estimated. Some experiments were also

(25) Ducker, W. A.; Senden, T. J.; Pashley, R. M. *Nature* **1991**, *353*, 239–241.

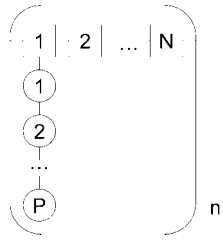

Figure 3. Schematic representation of the comb polymers considered. The polymer contains *n* segments, each with one side chain. Each side chain contains *P* monomers. Each segment contains *N* backbone monomers.

conducted at higher ionic strength by adding NaCl, 10 and 100 mM, to the polymer solutions.

In addition, for each polymer a representative curve is taken for full examination of the force−distance relation in regard to the theoretical predictions presented earlier.

III. Theory

In this section, we present a model for the conformation in solution and on surfaces of comb copolymers, as well as for the steric hindrance they develop when adsorbed layers of approaching surfaces overlap. For this, we first recall some well-established notions about linear polymers. After this, a more recent theory about comb homopolymers in solution[26] is presented and then extended to cover comb copolymers. This approach is then adapted to the adsorbed state before deriving the expression for steric hindrance.

These models are derived within a scaling law approach and, therefore, cannot be expected to provide very accurate numerical predictions. Nevertheless we attempt to calculate these factors as quantitatively as possible, while not overemphasizing their importance. Alternative models have also been examined. Their description and the reasons for which they were not selected are briefly mentioned in Appendix A.

III.1. Solution Conformation. *III.1.1. Linear Chain.* For a single polymer chain in a good solvent, the average end-to-end distance, R, can be obtained by minimizing the Flory free energy, A_F. The latter can be written as a sum of an elastic energy and an excluded volume energy term:[18,27,28]

$$\frac{A_F}{k_B T} = \frac{3}{2}\frac{R^2}{Pa^2} + Pv\frac{P}{R^3} \tag{2}$$

where a is the monomer size, P is the number of monomers in the chain, and v is the excluded volume that depends on the Flory parameter χ:

$$v = a^3(1 - 2\chi) \tag{3}$$

Minimization of eq 2 leads to

$$R = (1 - 2\chi)^{1/5} a P^{3/5} \tag{4}$$

III.1.2. Comb Homopolymers. In this section, we present the Gay and Raphaël[26] model for comb homopolymers in solution as a basis for interpreting our comb copolymer. In this model, the polymer backbone is defined as the assemblage of n repeating structural units, each containing N monomers and one side chain of P monomers (Figure 3). Five different types of conformations are then defined: decorated chain (DC), flexible backbone worm (FBW), stretched backbone worm (SBW), stretched backbone star (SBS), and flexible backbone star (FBS). These regimes are conveniently assembled into a phase diagram (Figure 4). However, the location of the boundaries is not exact because of the scaling nature of the approach.

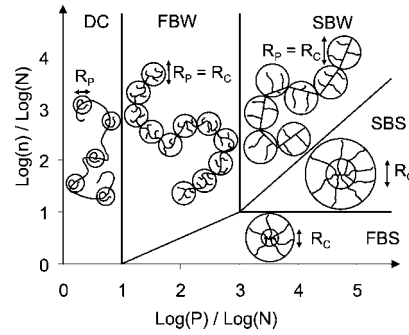

Figure 4. Phase diagram for comb homopolymers according to Gay and Raphaël (ref 26). The different domains are the following: decorated chains (DC), flexible backbone worm (FBW), stretched backbone worm (SBW), stretched backbone star (SBS), and flexible backbone star (FBS). R_C denotes core size, and R_p is side-chain size.

The polymers used in this study (Table 1) are in the FBW regime (although S10 is borderline with the FBS regime). For this type of conformation, the polymer can be viewed as a chain of cores, each having a radius of gyration of (actually average end-to-end distance) R_C, and the overall polymer radius of gyration R follows a Flory scaling law:[26]

$$R = R_C\left(\frac{n}{n_C}\right)^{3/5} \tag{5}$$

where n_C is the number of side chains (or segments) in a core.

Each core can be viewed as borderline case between the FBW and FBS. This imposes the condition that for each core

$$n_C^2 = \frac{P}{N} \tag{6}$$

which implies that the elastic energy of the side chains and the backbone section in the core are equal in a core.

The size of a core is obtained by minimizing its Flory energy:

$$\frac{A_F}{k_B T} = \frac{3}{2}\frac{R_C^2}{N_a^2} + \frac{3}{2}n_C\frac{R_C^2}{P_a^2} + n_C P v\frac{n_C P}{R_C^3} \tag{7}$$

This energy includes an elastic energy for both the backbone segment (first term) and one for the side chains (second term). The third term corresponds to the excluded volume energy of the side-chain segments in a core. Indeed, each of the $n_C P$ monomers feels an average concentration of order $n_C P/R_C{}^3$, hence having an excluded volume energy of order $v n_C P/R_C{}^3$. Multiplying the latter expression by the number of monomers, $n_C P$, leads to the desired expression.

Minimization of eq 7 and use of eq 6 lead to

$$R_C = \left(\frac{1 - 2\chi}{2}\right)^{1/5} a P^{3/5} n_C{}^{1/5} = \left(\frac{1 - 2\chi}{2}\right)^{1/5} a P^{7/10} N^{-1/10} \tag{8}$$

Substituting eqs 6 and 8 into eq 5, we find for the polymer radius of gyration

$$R = (1 - 2\chi)^{1/5} a P^{2/5} N^{1/5} n^{3/5} \tag{9}$$

III.1.3. Comb Copolymers. The derivation of eq 9 assumes a homopolymer. Provided one continues to assume good solvent conditions, it can be extended to include different monomer sizes in the backbone and in the side chains. We note a_N the backbone

(26) Gay, C.; Raphaël, E. *Adv. Colloid Interface Sci.* **2001**, *94*, 229–236.
(27) Flory, J. P. *Principles of Polymer Chemistry*; Cornell University Press: Ithaca, NY, 1953.
(28) Rubinstein M.; Colby, R. H. *Polymer Physics*; Oxford Press: Oxford, U.K., 2003.

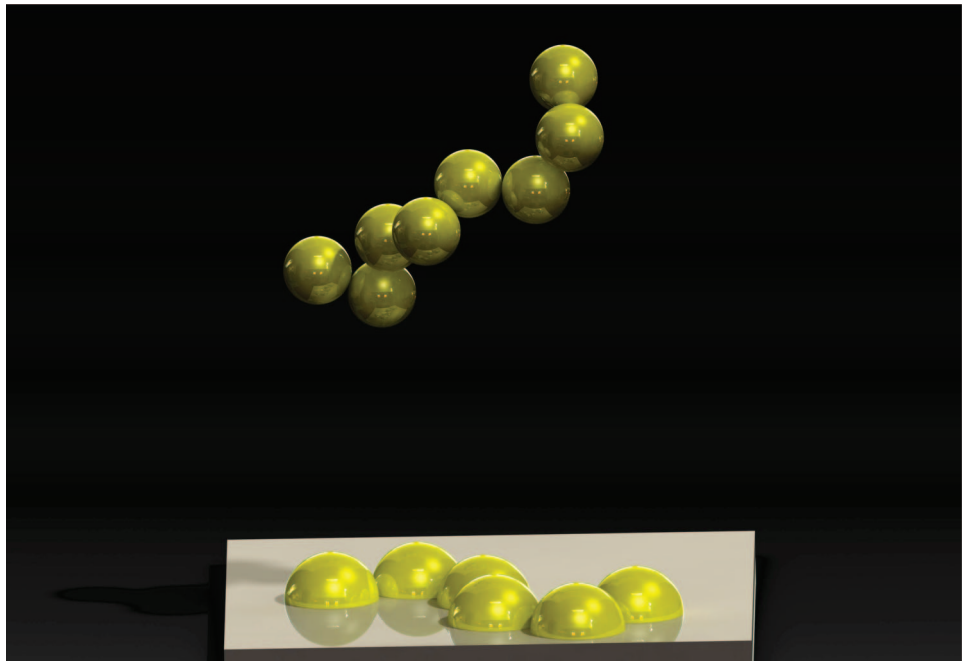

Figure 5. Schematic representation of a comb copolymer in solution (chain of spherical cores, each of radius R_C) and one adsorbed on a mineral surface (chain of hemispheres, each of radius R_{AC}).

monomer size and a_P the side-chain monomer size. The Flory energy is then written as

$$\frac{A_F}{k_B T} = \frac{3}{2}\frac{R_C^2}{n_C N a_N^2} + \frac{3}{2} n_C \frac{R_C^2}{P a_P^2} + n_C P a_P^3 (1-2\chi)\frac{n_C P}{R_C^3} \quad (10)$$

and eq 6 becomes

$$n_C^2 = \frac{P}{N}\left(\frac{a_P}{a_N}\right)^2 \quad (11)$$

which leads to

$$R_C = \left(\frac{a_P}{a_N}\frac{(1-2\chi)}{2}\right)^{1/5} a_P P^{7/10} N^{-1/10} \quad (12)$$

for the radius of gyration of the core in place of eq 8. The polymer radius of gyration is

$$R = \left(\left(\frac{a_N}{a_P}\right)^2 \frac{(1-2\chi)}{2}\right)^{1/5} a_P P^{2/5} N^{1/5} n^{3/5} \quad (13)$$

In this paper, polymers have a methacrylate backbone (a_P = 0.25 nm) and poly(ethylene oxide) (PEO) side chains (a_N = 0.36 nm). Also, according to a recent neutron scattering study, the value of χ for PEO is about 0.37 at 25 °C.[29] This value is preferred to others, because the authors accounted explicitly for the semidilute regime of their solutions in their scattering data analysis.

III.2. Surface Conformation. It is indicated that these comb copolymers adsorb on cementitious materials because of ionic interaction between their backbones and the surfaces.[4,6,8,10] The polymer must therefore reorganize itself for the backbone to get close to the surface. Our assumption is that this situation can be treated similarly to the FBW in solution, using a chain of hemispheres on a surface (Figure 5). The size and number of these hemispheres are derived in an analogous way to the size and number of cores in solution.

The radius of these hemispheres is noted R_{AC}. The different contributions to their Flory energy are treated in a similar way to eq 10, but with different characteristic dimensions for each term. For the surface elastic energy of the backbone we use R_{AC} (dimension parallel to the surface). For the side chains, we take the geometrical mean between dimensions parallel (R_{AC}) and perpendicular ($R_{AC}/2$) to the surface. For the excluded volume energy we use the volume of the hemisphere.

The Flory free energy for each core is then written as

$$\frac{A_F}{k_B T} = \frac{3}{2}\frac{R_{AC}^2}{n_{AC} N a_N^2} + \frac{3}{2} n_{AC} \frac{(R_{AC}^2/2)}{P a_P^2} + n_{AC} P \upsilon \frac{n_{AC} P}{(R_{AC}^3/2)} \quad (14)$$

where the subscript AC instead of C refers to the fact that these are adsorbed cores. For simplicity, we neglect the contribution of the excluded volume of the backbone as well as the role of adsorption energy.

As for the solution case, we assume that the equality between the elastic energies of the side chains and the main chain segment in a given core defines the number of side chains n_{AC} in this core (hemisphere):

$$n_{AC} = \frac{a_P}{a_N}\left(2\frac{P}{N}\right)^{1/2} \quad (15)$$

Free energy minimization of eq 14 and use of eq 15 leads to

$$R_{AC} = \left(2\sqrt{2}(1-2\chi)\frac{a_P}{a_N}\right)^{1/5} a_P P^{7/10} N^{-1/10} \quad (16)$$

The surface occupied by each molecule can be calculated for a dense packing in a similar way as for eq 40 in Appendix A, giving

$$S = \frac{\pi}{\sqrt{2}} a_N a_P \left(2\sqrt{2}(1-2\chi)\frac{a_P}{a_N}\right)^{2/5} P^{9/10} N^{3/10} n \quad (17)$$

III.3. Steric Hindrance. When two surfaces approach enough for their adsorbed layers to overlap, a steric force develops. As this happens, the polymer cores are assumed to maintain their

(29) Pedersen, J. S.; Sommer, C. *Prog. Colloid Polym. Chem.* **2005**, *130*, 70–78.

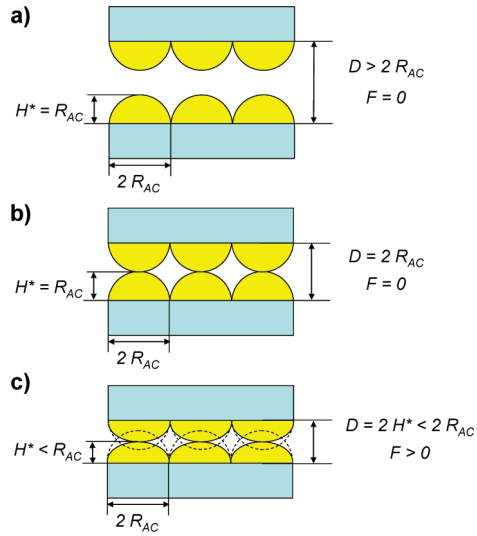

Figure 6. Schematic illustration of the steric hindrance hypothesis: (a and b) layers do not overlap, the adsorbed core dimensions are not changed, and the force is zero; (c) the layers could overlap (discontinuous lines), instead they get compressed; they maintain a lateral dimension of $2R_{AC}$, but their vertical dimension is reduced and equal to $D/2$, which is also H^*.

lateral dimension, but the distance perpendicular to the surface, now noted H^*, can decrease. This is supported by the fact that the surface coverage by the polymers is very high (the value of f_S given in eq 25 is very close to unity). As a result there is little free space between the polymers, which would imply that lateral spreading (extension) of the cores would not be favored, because cores would begin to overlap (Figure 6).

The Flory energy of a given core is rewritten introducing H^* to get an expression analogous to eq 14:

$$\frac{A_F}{k_BT} = \frac{3}{2}\frac{R_{AC}^2}{n_{AC}Na_N^2} + \frac{3}{2}n_{AC}\frac{R_{AC}^{4/3}H^{*2/3}}{2Pa_P^2} + a_P{}^3(1-2\chi)\frac{2n_{AC}^2P^2}{H^*R_{AC}^2} \tag{18}$$

The derivative of this expression with respect to the volume change upon approach is the osmotic pressure ϕ, which is also the force per unit area of a polymer core. As was mentioned earlier, the condition expressed by eq 15 means that for FBWs, the first two terms are equal. We assume the same remains true under compression, so differentiation leads to

$$\varphi = \frac{\partial(A_F/k_BT)}{\pi R_{AC}^2\,\partial H^*} = \frac{P^{-29/30}N^{-13/30}}{\alpha_{2D-FBW}}H^{*-1/3}\left[1-\left(\frac{R_C}{H^*}\right)^{5/3}\right] \tag{19}$$

where

$$\alpha_{2D-FBW} = \pi 2^{-3/10}a_P^{5/3}a_N\left((1-2\chi)\frac{a_P}{a_N}\right)^{2/15} \tag{20}$$

To go from the interaction force per unit area between flat plates (eq 19) to the force between spheres of different sizes, one can use the Derjaguin approximation. This basically requires that the radius of either sphere be much larger than the surface-to-surface separation h. The total force is then obtained by integrating the force of opposite circular sections on the two spheres. The integration is carried out between the separation distance of interest D and $2R_{AC}$, which is when the force is zero.

$$\frac{F}{k_BT} = 2\pi\left(\frac{R_1R_2}{R_1+R_2}\right)\frac{P^{-6/5}N^{-2/5}}{\alpha}\int_D^{4R_{AC}}H^{*-1/3}\left(1-\left(\frac{R_{AC}}{H^*}\right)^{5/3}\right)dh \tag{21}$$

Carrying out the integral leads to

$$\frac{F}{k_BT} = 2\pi\left(\frac{R_1R_2}{R_1+R_2}\right)\frac{P^{-29/30}N^{-13/30}}{\alpha}\left(\frac{5}{2^{1/3}}R_{AC}{}^{2/3} - \frac{1}{2}D^{-1/3}\times\left(3D+4(2^{2/3})\,R_{AC}\left(\frac{R_{AC}}{D}\right)^{2/3}\right)\right) \tag{22}$$

For our AFM experiments, the cantilever tip is interacting with a flat surface ($R_2 = \infty$). Assuming the cantilever tip end is hemispherical, with a radius of R_{tip}, we get

$$F = \beta\left(\frac{5}{2^{1/3}}R_{AC}^{2/3} - \frac{1}{2}D^{-1/3}\left(3D+\ 4(2^{2/3})R_{AC}\left(\frac{R_{AC}}{D}\right)^{2/3}\right)\right) \tag{23}$$

with

$$\beta = \frac{2\pi k_BTR_{tip}}{\alpha}P^{-29/30}N^{-13/30} \tag{24}$$

IV. Results

IV.1. Imaging. Prior to adding the polymer, the surfaces were imaged and the forces measured. A typical image is shown in Figure 7, where some porosity can be seen along with smooth zones.

At short separation distance, the force among these surfaces becomes slightly attractive but is then much more attractive upon pullout. The origin of this strong interparticle force has been attributed to ion correlation forces.[12,18] A typical curve in absence of superplasticizers is shown in Figure 8.

In the presence of superplasticizer the surface topology changes to an extent that depends on the type and amount of polymers. However, there is generally little difference between the curves obtained at 5 and 10 mg/L, indicating the existence of surface saturation. For this reason and with the purpose of mainly evaluating properties at full surface coverage, we report mainly data at 10 mg/L. An example of images obtained in presence at this dosage at 10 mg/L for two different polymers is shown in Figure 9.

A general feature of such images is the presence of some porous patches. These vary depending on the nature of the polymer, as can be seen in the two cases illustrated in Figure 9.

IV.2. Layer Thickness. This surface porosity is of little use in terms of determining the layer thicknesses and surface forces. Indeed, the difference between the maximum and the minimum on surface roughness mapping is not adequate for estimating

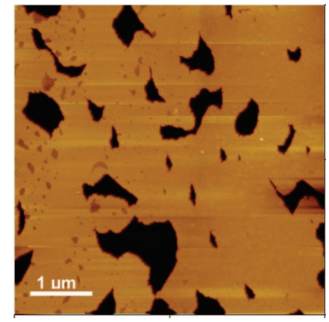

Figure 7. Typical topographical image of a C−S−H substrate in absence of superplasticizer. Image size: 5 μm. Relative height: 100 nm.

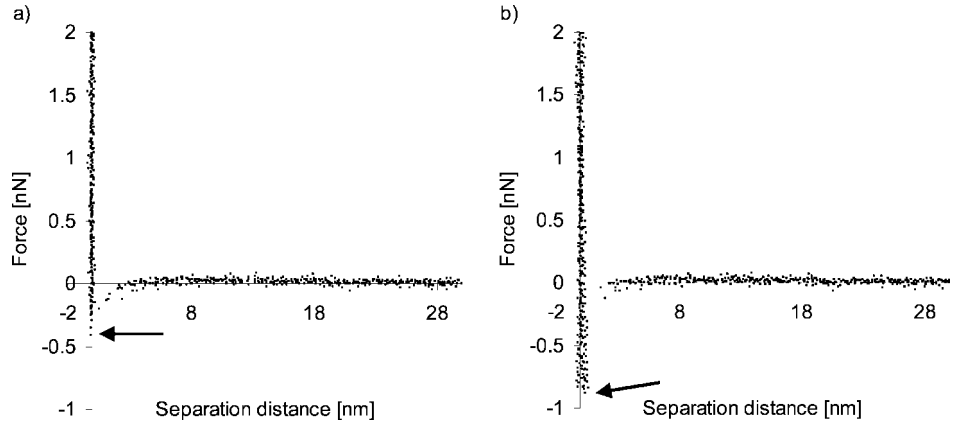

Figure 8. Typical force curve between C−S−H nanoparticles in the absence of superplasticizer: (a) curve upon approach; (b) curve upon separation. The arrows indicate the magnitude of the adhesion force.

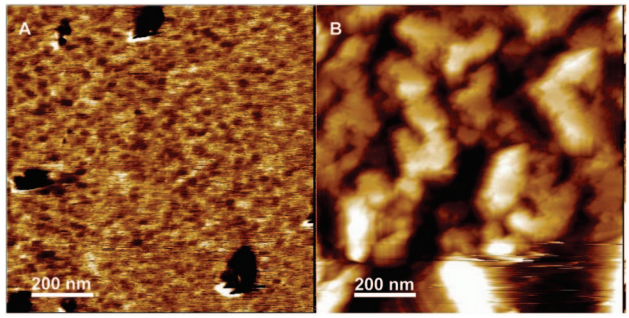

Figure 9. Images ($1 \times 1\ \mu m^2$) (topography on left, error signal on right) of a C−S−H substrate in the presence of superplasticizer dosed at 10 mg/L: (A) S3 (side chains of 1000 g/mol); (B) S10 (side chains of 10 000 g/mol); relative height, 100 nm.

polymer layer thickness, since the depth of the valleys may be substantially lower than the layer thickness. Rather, values are obtained more reliably from the force−distance curves.

Indeed, in presence of adsorbed polymers such curves are generally repulsive, although in some cases they may show an attracto−repulsive behavior at low dosage. Pedersen and Bergström, for instance, estimated the layer thickness of adsorbed linear polyelectrolytes by colloidal probe AFM measurements.[30] More specifically, by varying the ionic strength of the liquid phase they could divide these curves into a steric (short-range) and an electrostatic (long-range) part. In our case the repulsion was predominantly steric, since increase in the ionic strength by including additional 1, 10, and 100 mM NaCl to the 5 mM $Ca(OH)_2$ solution did not change the force−distance curves much.

An illustration of typical force−distance curves upon approach for two polymers at 10 mg/L is given in Figure 10. The different distances at which the force becomes repulsive are quite obvious between the polymer with short side chains (S3, 1000 g/mol) and the one with long side chains (S10, 10 000 g/mol). The filled circle marks the separation distance we use as the onset of adsorbed layer overlap, estimated visually. As is explained in the Discussion section, an average proportionality constant can be defined by comparison between measured values and those predicted by eq 25. Calculated values including this correction are reported in Table 2 along with the measured values.

IV.3. Steric Hindrance. The accuracy of eq 23 to predict the dependence of steric hindrance on separation distance has been tested by using the experimentally determined value of layer thickness and adjusting the values of β to get the best fit to experimental data. Doing this, it was found that results improved very much if the layer thicknesses are incremented by the maximum compression value. It is assumed that layers cannot be compressed below this value and that this causes an offset in the reported separation distance. This observation is in agreement with other colloidal probe measurements reported in the literature.[30]

In absence of a good way to determine this additional parameter independently, it was initially treated as an additional adjustable parameter, δ_0 (maximum compression thickness). Each curve was therefore fitted by adjusting both δ_0 and β, the force prefactor. Doing this, we found that for 9 out of 10 polymers, δ_0 was between 0.5 and 1 nm. For this reason and to reduce the overall extent of fitting, the average value of δ_0 over these nine polymers (0.78 nm) was then used for all polymers. This means that in a second stage all force curves were adjusted only by varying β. This leads to a good agreement with experiment as illustrated in Figure 10. The theoretical values, after correction by the proportionality factor f_β (see discussion), are reported in Table 2 along with the measured values.

V. Discussion

In section III, a treatment for the comb copolymer conformation in solution and on surfaces was presented. In addition, expressions predicting the layer thickness (eq 16) and the steric hindrance as a function of separation distance (eq 23) were derived.

In section IV, basic results of our AFM colloidal probe investigations on such comb copolymers were presented. It was shown that force curves could be well fitted by the theory if the existence of a maximum degree of compression is introduced. This parameter can be taken identical for all polymers so that the degree of fitting is greatly reduced. Since the layer thickness comes from the point at which the force deviates from the baseline, only one parameter, β, is then needed to adjust each force curve.

In this section, we examine whether the values of the adjusted parameters (δ and β) are consistent with the model predictions, in particular, in terms of molecular structure. We begin with the solution conformation and surface coverage for which data available in the literature is used.

V.1. Solution Conformation. In solution, it is expected that the end-to-end distance should be proportional to the hydrodynamic or radius of gyration. Borget et al.[31] and Houst et al.[32] report such data for comb copolymers similar to ours and that

(30) Pedersen, H. G.; Bergström, L. *J. Am. Ceram. Soc.* **1999**, *82*(5), 137–1145.

(31) Borget, P.; Galmiche, L.; Le Meins, J.-F.; Lafuma, F. *Colloids Surf., A* **2005**, *260*, 173–182.

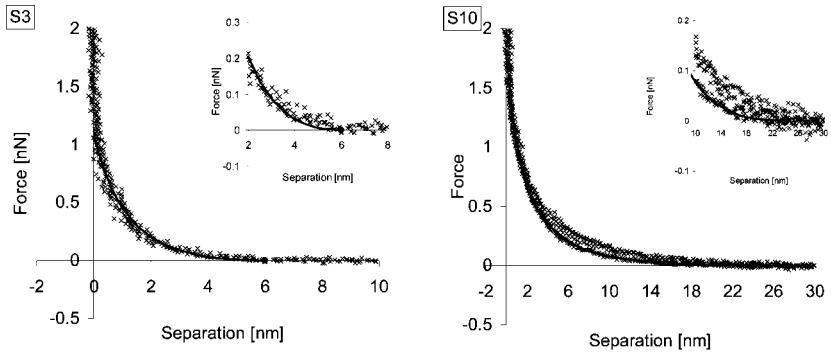

Figure 10. Force−distance curves. The dots show data from five different runs. The continuous lines show the fit obtained with eq 23 and using the measured layer thickness reported in Table 2. S3 has side chains of 1000 g/mol, and S10 has side chains of 10 000 g/mol. The large circles indicate the estimated values at which the polymer layers begin to overlap (twice the layer thickness). The insets show a magnification in the zone where layer thickness values are determined.

Table 2. Structural Parameters of the Comb Copolymers and Values of Calculated Layer Thickness and Force Prefactor (β)[a]

	structural parameters			layer thickness		force prefactor		
name	P	N	n	calc nm	meas nm	calc nN	meas nN	Adsorbed cores no.
S1	13	3	23	2.7	3.6	0.208	0.122	5.6
S2	17	3.5	20	3.3	3.9	0.144	0.111	4.5
S3	23	3.3	25	4.0	3.8	0.112	0.100	4.6
S4	23	4.1	85	3.9	4.8	0.102	0.076	17.9
S5	23	9.25	18	3.6	5.3	0.072	0.048	5.6
S6	45	4	15	6.4	4.6	0.053	0.047	2.3
S7	45	7.4	9	6.0	6.8	0.040	0.042	1.9
S8	114	7.7	11	11.4	8.8	0.016	0.029	1.4
S9	114	14	12	10.8	8.8	0.013	0.013	2.2
S10	227	22	4	16.7	12.8	0.005	0.015	0.6

[a] The calculated values are given after correction by the factors f_δ and f_β (see section V, eqs 28 and 30). The last column gives the number of adsorbed cores (hemispheres).

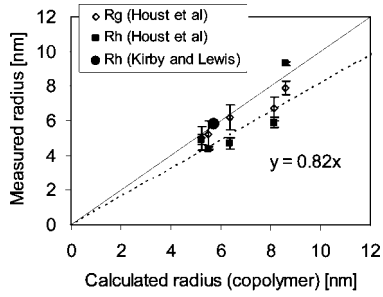

Figure 11. Correlation between the end-to-end distance from eq 13 and the experimentally obtained gyration and hydrodynamic radii (refs 10, 31, and 32). The continuous line is the diagonal, and the discontinuous one is the best fit to all the data (forced through the origin).

are also in the FBW regime. Data for one additional such copolymer is also given by Kirby and Lewis[10] (their two other comb copolymers are not FBW). These data are plotted in Figure 11 versus the end-to-end distance obtained from eq 13, and a good correlation is found.

V.2. Surface Coverage. Adsorption data of comb copolymers similar to ours are given by Perche for suspensions of MgO.[17,21] In his experiments, Perche let the suspensions evolve for 30 min, during which the surface of the powder reacted and the specific surface increased. After that, he showed that there was only a very slow evolution of the specific surface. By adding the polymer at that time, adsorption could be measured on a nonreactive suspension, of which the specific surface was 7.53 m^2/g.[17,21] Using these data and neglecting the role of surface roughness, we determine the surface occupied by each polymer.

However, we are operating within a scaling approach, so there is an uncertainty on numerical prefactors. To overcome this, we introduce $r_{S,i}$, the ratio between calculated and measured surfaces occupied by a polymer ($S_{calc,i}$ and $S_{exp,i}$), which is furthermore normalized by the geometrical mean of the same ratio:

$$r_{S,i} = \frac{S_{calc,i}/S_{exp,i}}{f_S} \tag{25}$$

where f_S is the surface coverage normalization factor give by the geometrical mean of $S_{calc,i}/S_{exp,i}$:

$$f_S = \sqrt[n_i]{\prod_{i=1}^{n_i} S_{calc,i}/S_{exp,i}} \tag{26}$$

In this way values of $r_{S,i}$ are centered on unity, and the quality of the fit can then judged by the data scatter around this value. In a second stage, the value of f_S is considered. We refer to it as the surface coverage normalization factor. The closer it is to unity, the better would be the absolute match of the model to the experiment.

In Figure 12, we plot values of $r_{S,i} - 1$. They indicate the relative error of eq 17 after normalization by f_S. Although one sample shows a rather larger error (45%), all other errors are relatively small. In fact these are all amplified because of dealing with a surface rather than a single dimension. For example, if the calculated surfaces are brought back to single polymer dimension, then the largest error reduces to only 20%, which is quite satisfactory.

(32) Houst, Y. F.; Bowen, P.; Perche, F.; Kauppi, A.; Borget, P.; Galmiche, L.; Le Meins, J.-F.; Lafuma, F.; Flatt, R. J.; Schober, I.; Banfill, P. F. G.; Swift, D. S.; Myrvold, B. O.; Petersen, B. G.; Reknes, K. *Cem. Concr. Res.*, in press.

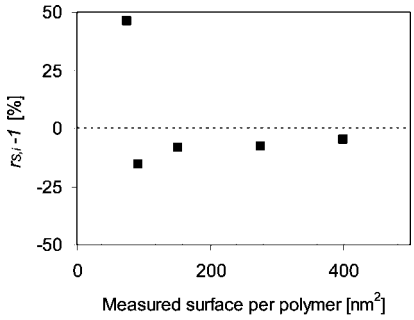

Figure 12. Normalized ratio of calculated to measured area occupied by a comb copolymer on MgO (values calculated from Perche (ref 21), Kjeldsen et al. (ref 17), and Houst et al. (ref 32).

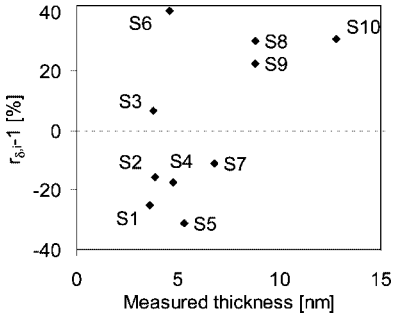

Figure 13. Relative error of the normalize layer thickness calculation.

This indicates that eq 17 includes adequate exponents for the molecular structure parameters P, N, and n. The quantitative accuracy is also rather good since f_S is close to unity (1.13).

V.3. Layer Thickness. As indicated in section IV, adjusting the force curves led to the conclusion that the separation distance was biased by a fixed distance corresponding to twice the maximum compression of a polymer layer, δ_0. To reduce the extent of fitting, a fixed average value was used for all polymers (0.78 nm). The visual estimate of the layer thickness must therefore by incremented by δ_0.

To evaluate the accuracy of layer thickness estimation by eq 25, we use a similar approach as above is used. A normalized ratio between calculated, and measured layer thickness is used:

$$r_{\delta,i} = \frac{\delta_{\mathrm{calc},i}/\delta_{\mathrm{exp},i}}{f_\delta} \tag{27}$$

where f_δ is the layer thickness normalization factor given by

$$f_\delta = \sqrt[n_i]{\prod_{i=1}^{n_i} \delta_{\mathrm{calc},i}/\delta_{\mathrm{exp},i}} \tag{28}$$

Values of the normalized relative error ($r_{\delta,i} - 1$) are given in Figure 13. Of the 10 polymers, one has an error slightly above 40%, whereas the remaining nine polymers are all below 32%. This means that eq 16 has adequate exponents for P, N, and n. It therefore captures well the main parameters of the molecular structure. The quantitative accuracy is also good since f_δ. is close to unity. It is, however, not extremely accurate since its value is of 0.71.

V.4. Steric Hindrance. The good fits shown in Figure 10 indicate that eq 23 correctly accounts for the variation of the steric force with separation distance. However, it does not state whether the dependence on molecular structure is correct. In fact, it must be at least correct in part, since it includes the layer thickness and that parameter is well predicted (in scaling terms).

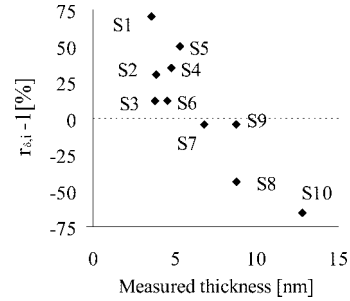

Figure 14. Relative error of the normalized value of β.

In addition, we must check if the values of β obtained by the fit are consistent with those predicted with eq 24. As in the previous cases, we use an additional normalized ratio:

$$r_{\beta,i} = \frac{\beta_{\mathrm{calc},i}/\beta_{\mathrm{meas},i}}{f_\beta} \tag{29}$$

where f_β is the steric hindrance normalization factor

$$f_\beta = \sqrt[n_i]{\prod_{i=1}^{n_i} \beta_{\mathrm{calc},i}/\beta_{\mathrm{meas},i}} \tag{30}$$

This time, errors are larger as shown in Figure 14. However, it is interesting to observe that the largest errors come from polymers S1 and S10 that have, respectively, the shortest and largest side chains. In fact, S10 is a borderline case between FBW and FBS conformations. Moreover, its number of adsorbed cores (n/n_{AC}) is smaller than one (Table 2), indicating that in the adsorbed state it is closer to the FBS than to the FBW regime. Interestingly, the polymer that has the next lowest number of adsorbed cores is S8 (Table 2) and it also shows a clear difference from the rest of the predictions (Figure 14). If these two polymers are left out of the analysis, we find that all errors are then within less than 25%, apart for S1, which is slightly lower than 40%. In this case, the reason may be that the side chains are too short for our treatment to be applicable. Given these restrictions to the applicability of our model to the cases of polymers S1, S8, and S10, it appears that eq 24 includes adequate exponent for P, N, and n. It implies that this model captures the role of molecular structure of comb copolymers on steric hindrance well provided they adopt a flexible backbone worm analogue conformation.

In terms of the quantitative accuracy, we examine the value of the steric hindrance normalization factor, f_β. This depends on the tip radius, R_{tip}, which is not known very accurately. Because of this, we calculate the tip radius needed for f_β to be unity (perfect prediction). This turns out to be 15 nm but must be corrected because of the inaccurate estimate of the polymer dimension revealed in the layer thickness evaluation ($f_\delta = 0.71$). Assuming that this error comes from the persistence length of both the side chains and the backbone, a correction of $f_\delta^{-8/3}$, must be used. It leads to a tip radius of 38 nm instead of 15 nm. This is substantially below the 100 nm that can be estimated based on measurements by Plassard[33] (Plassard's data and analysis for the plate-on-plate configuration is translated to the case of sphere on plate). However, this value is itself not accurate since it is based on an estimate of the minimum separation distance (in fully dry conditions and in absence of polymer). This was taken to be 0.2 nm. The estimated error of ± 0.1 nm would mean the tip size could be between 25 and 230 nm so that the difference in estimated tip radii must not be given too much importance.

It should also be noted that the surface coverage could be lower than we have assumed based on the experiments on MgO.

In fact, the adsorbed cores cannot fully cover the surface as we assumed. On the basis of the random packing of spheres on a surface,[34] an additional correction factor of 1.2 would have to be included (bringing the radius to 45 nm). However, since these cores are linked in a given polymer this value would be higher. Finally, we are inevitably bound by the limitations of the scaling law approach that cannot deliver accurate numerical factors. In summary, this means that the mismatch of the tip radius does not compromise the overall result. Most importantly, we can state that the role of all structural parameters of these comb copolymers in steric hindrance seem to be correctly situation that has been considered in the derivation.

VI. Conclusions

The layer thickness of polycarboxylate superplasticizers adsorbed onto C−S−H has been measured. Results show that the superplasticizer adsorption cancels the strong ion correlation forces that exist between surfaces at close separation.

It has been shown that in solution the conformation of our comb copolymers can be well accounted for by a scaling law approach extracted from Gay and Raphaël's model.[26] Extension of this model to an adsorbed comb copolymer accounts well for the surface occupied by individual polymers as well as for the layer thickness thereof. Furthermore, the force−distance relationship for such adsorbed conformation was derived and found to account very well for the variation of steric hindrance with separation distance. It was also found to account well for the main molecular parameters such as grafting density and side-chain and backbone length. The adsorption conformation of these polymers and their steric hindrance therefore appear to be well described by the model presented in this paper.

Acknowledgment. E.R. and R.J.F. thank Dr. Jean-Baptiste d'Espinose for very useful discussions on the topic of comb copolymer conformation.

Appendix A

Alternative models may be considered for the surface conformation of these polymers.

1. Mushroom

In the case of an end-anchored chain, not interacting with its neighbors, we have a so-called mushroom conformation. The classical treatment[35] states that the layer thickness should be on the order of R_F, the Flory radius of the polymer in solution. It derives a segment density as a power law (two-thirds) of distance valid up to the distance R_F, beyond which it is stated that the segment density decreases rapidly.

The same paper also states earlier that the mushroom conformation can be assimilated to a hemisphere with a radius close to the R_F. Here we elaborate that statement somewhat more. We consider a sphere with the same radius as the mushroom and note it R_m. We then assume that the characteristic dimension for the elastic energy term is the geometrical mean between the dimension parallel to the surface (R_m) and the one perpendicular to it ($R_m/2$). The volume taken for the excluded volume energy is based on a hemisphere of radius R_m. We then get

$$\frac{A_F}{k_B T} = \frac{3}{2}\frac{(R_m^2/2)}{P_a^2} + \frac{P^2 \upsilon}{(R_m^3/2)} \tag{31}$$

Minimization of the free energy leads to

$$R_m = 2^{2/5}(1-2\chi)^{1/5} a P^{3/5} \tag{32}$$

The similarity with eq 2 shows that the general mushroom size indeed scales in the same way as the radius of gyration of the polymer in solution.[18,35] Furthermore the additional numerical factor suggests the layer thickness of a mushroom would be about 30% larger than the radius of gyration of the same polymer in solution, R_F, as implied by the classical treatment. For the mushroom model, the value of R_m is taken as the distance between the polymers.[17]

2. Mushroom Slices

An alternative approach that remains at the single side-chain level is also worth presenting. It considers that each of the n segments (N backbone units and one side chain) can be assimilated to a *mushroom slice* with a thickness D and radius R_S. The side chain is then modeled as a sequence of blobs of size D, which is obtained assuming the backbone section adopts a 2D Flory radius of gyration so that

$$D = a_N N^{3/4} \tag{33}$$

Each blob then contains g monomers and fulfills the condition

$$g = \left(\frac{a_N}{a_P}\right)^{5/3}(1-2\chi)^{-1/3} N^{5/4} \tag{34}$$

The Flory energy for the 2D chain of such blobs is then written in an analogous way to eq 31:

$$\frac{A_F}{k_B T} = \frac{3}{2}\frac{(R_S{}^2/2)}{D^2 B} + \frac{B^2 D^2}{(R_S{}^2/2)} \tag{35}$$

where B is the number of blobs given by P/g. Minimization of the free energy leads to

$$R_S = \left(\frac{8}{3}\right)^{1/4} D\left(\frac{P}{g}\right)^{3/4} \tag{36}$$

which together with eqs 33 and 34 gives

$$R_S = \left(\frac{8}{3}\right)^{1/4}\left(\frac{a_P}{a_N}\right)^{1/4}(1-2\chi)^{1/4} a_P P^{3/4} N^{-3/16} \tag{37}$$

The surface occupied by each molecule would then be written as

$$S = nDR_S = \left(\frac{8}{3}\right)^{1/4}\left(\frac{a_P}{a_N}\right)^{1/4}(1-2\chi)^{1/4} a_N a_P P^{3/4} N^{9/16} n \tag{38}$$

3. Deposited FBW

The simplest extension of the FBW conformation to the adsorbed state assumes that the core sizes remain unchanged from solution. The deposited chain of cores would then adopt a 2D Flory radius on the surface, as opposed to the 3D one it had in the solution. Under this assumption, the layer thickness would be equal to twice the radius R_C, given in eq 12, and the radius of gyration of the polymer on the surface would be

$$R_{2D} = R_C\left(\frac{n}{n_C}\right)^{3/4} \tag{39}$$

The surface occupied per adsorbed molecule would be proportional to the square of this value if polymers effectively exclude each other from their own surrounding. Alternatively, in the extreme case of close packing, the surface per adsorbed molecule can be expected to be

$$S = \pi\left(\frac{n}{n_C}\right)R_C{}^2 = \pi(a_N a_P)\left(\frac{a_P}{a_N}\frac{(1-2\chi)}{2}\right)^{2/5} P^{9/10}N^{3/10}n \quad (40)$$

Here the choice of the end-to-end distance as the radius of the area occupied is guided by the result in Figure 11 that shows the polymer hydrodynamic and radius of gyration to be almost equal to this distance. We assume the same is true at the core scale.

4. Value of Alternative Models

These alternative models capture the layer thickness and surface coverage with similar accuracy to the model presented in this paper. However, from a physical point of view the mushroom model is not credible because side chains are too close together. The FBW deposition would not allow interaction of the ionic group with the surface so that there would no enough driving force for adsorption. The mushroom slice model is generally more credible but overall performs less well than the model presented in this paper. The above equations are given in case they may be of use in other systems.

LA801410E

(33) Plassard, C. Etude fondamentale des mécanismes à l'origine de la cohésion des nanoparticules de silicates de calcium hydrates par microscopie à force atomique. Ph.D. thesis, University of Bourgogne, 2005.
(34) Berryman, J. G. *Phy. Rev. A* **1983**, *27*, 1053–1061.
(35) De Gennes, P.-G. *Macromolecules* **1980**, *13*, 1069–1075.